Int. J. Therm. Sci. (2000) 39, 236–248

S1290-0729(00)00242-8/FLA

Alterations to coherent flow structures and heat transfer due to pulsations in an impinging air-jet

Emilia-Cerna Mladin [a]*, David A. Zumbrunnen [b]

[a] *UNESCO Chair of Engineering Sciences, Politehnica University, Spl. Independentei 313, Bucharest, 77206, Romania*

[b] *Department of Mechanical Engineering, Clemson University, Clemson, SC 29634-0921, USA*

(Received 21 September 1998, accepted 7 July 1999)

Abstract — An investigation was carried out to study the effect of flow pulsation on the characteristics of a planar air jet impinging normally on a heated surface. Such information was further utilized to determine the influence of flow characteristics in the plane of impingement on Nusselt number distribution. Time-resolved system properties were investigated with modern instrumentation that allowed instantaneous heat transfer and flow velocity measurements to be performed simultaneously. Based on good coherence function estimates between the signals, heat transfer measurements were used in return to infer flow dynamics near the impingement surface. Experiments were performed for steady and pulsating jets at jet Reynolds numbers of 1 000, 5 500, and 11 000, pulse frequencies up to 82 Hz (corresponding to Strouhal numbers below 0.13), and pulse amplitude at the nozzle exit up to 50 % of the mean flow velocity. Special techniques commonly used for periodically disturbed flow fields elucidated the dynamics of the pulse and associated coherent flow structures. Results indicated the parametric conditions for which alterations are expected in time-averaged heat transfer from the surface. Engineering applications include cooling of electronic packages and heat transfer to gas turbine blades. © 2000 Éditions scientifiques et médicales Elsevier SAS

pulsed flows / submerged jets / coherent structures / transient heat transfer

Nomenclature

A	flow pulse amplitude $= \widetilde{V}_{\mathrm{rms}}/\overline{V}$, equation (3b)	
A_T	amplitude of periodic surface temperature component $= \widetilde{T}_{\mathrm{s,rms}}/\overline{T}_{\mathrm{s}}$	
A_q	amplitude of periodic surface heat flux component $= \tilde{q}_{\mathrm{s,rms}}/\bar{q}_{\mathrm{s}}$	
c	vortex/pulse advection velocity	$\mathrm{m\cdot s^{-1}}$
f_{ex}	excitation/pulsation frequency	Hz
h	convective heat transfer coefficient . . .	$\mathrm{W\cdot m^{-2}\cdot K^{-1}}$
H	nozzle-to-plate separation distance . . .	m
k_{f}	thermal conductivity of fluid	$\mathrm{W\cdot m^{-1}\cdot K^{-1}}$
Nu_w	Nusselt number $= hw/k_{\mathrm{f}}$	
q_{s}	convective surface heat flux	$\mathrm{W\cdot m^{-2}}$
Pr	Prandtl number	
Re_w	Reynolds number $= w\overline{V}_{\mathrm{N}}/\nu_{\mathrm{f}}$	
St_w	Strouhal number $= wf_{\mathrm{ex}}/\overline{V}_{\mathrm{N}}$	
t	time	s
T_{j}	jet temperature	K
T_{s}	surface temperature	K
Tu	turbulence intensity, equation (3a)	
V	jet flow velocity in the y_{N}-direction . .	$\mathrm{m\cdot s^{-1}}$
w	nozzle width	m
x	distance from the stagnation line, *figure 2*	m
y_{N}	downstream distance from the nozzle exit, *figure 2*	m

Greek symbols

φ	normalized phase associated with the velocity waveform	
λ	wavelength between subsequent vortices	m
ν	kinematic viscosity	$\mathrm{m^2\cdot s^{-1}}$

Subscripts

avg	time-averaged value
f	pertaining to film temperature $(T_{\mathrm{s}} + T_{\infty})/2$
N	pertaining to nozzle exit
S	pertaining to stagnation line ($x = 0$)
x	in the x-direction (*figure 2*)

* Correspondence and reprints.
cerna@fun.unesco.pub.ro

Superscripts

— arithmetic mean
~ periodic component with zero mean

1. INTRODUCTION

The jets impinging on heated surfaces have a free-jet region up to 80 % of the nozzle-to-plate distance, and its characteristics are carried on in the subsequent stagnation and wall jet regions [1]. There is a general agreement that the presence and interaction of the largest coherent structures that are generated naturally and nearly periodically dominate the behavior of a turbulent flow. A high-speed photograph technique was previously used to show that, in an unforced planar jet, vortices form either symmetrically (as illustrated in *figure 1*) or alternately about the nozzle centerline and decay after merging to yield larger vortices [2]. It has been shown that an external periodic disturbance (e.g., of acoustic nature or mechanically produced) enlarges selected coherent structures and organizes the somehow random structure formation and interaction characteristic of an unforced turbulent flow. Investigations on axisymmetric air jets with periodic oscillations in the fluid velocity indicated that the turbulence intensities along the jet axis increased at a faster rate and to higher saturation values than in steady jets [3]. Periodic fluctuations were amplified over a distance of two to three nozzle diameters but were essentially abated at a distance of ten diameters from the nozzle opening. The pulse decay was accompanied by a large increase in turbulence intensity as energy was transferred from periodic flow structures to turbulent motion. In periodically disturbed planar jets, high-speed photographs showed a sharper flow expansion very near the nozzle exit [4]. In addition, a cyclic generation of vortex structures was indicated at the nozzle exit, which subsequently traveled downstream. A past work on forced mixing layers reported that the vortex merging was suppressed for quite a long distance in the presence of a forcing frequency higher than about half of the most amplified natural frequency in the flow [5]. High-speed photographs indicated that the suppression of vortex merging inhibited the spreading of the mixing layer. The layer thickness was decreased with increasing frequency. A means was thus suggested to control the thickness of the layer with a forcing frequency.

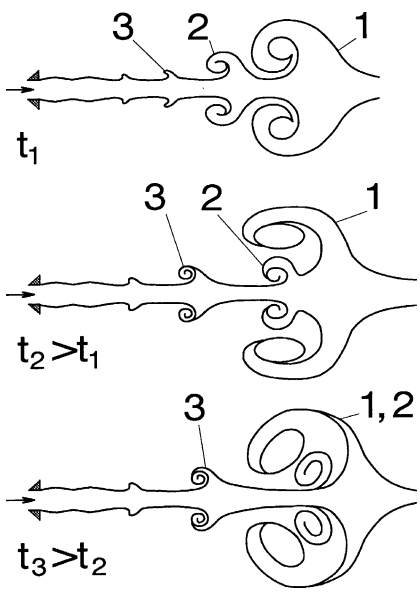

Figure 1. Vortex formation and pairing.

Previous works documented that a vortex merging event acts as a source for feedback in the flow. Low frequency modulations present on the instability wave near the nozzle of a free jet were found to match the vortex passage frequency at the end of the potential core [6]. They were attributed to upstream-propagating flow perturbations produced by the downstream vortex merging. The feedback equation states that the number of waves in a feedback loop should be an integer, implying that the location of vortex merging is determined globally. Moreover, the downstream-traveling coherent structures and the upstream propagating vorticity waves are locked in phase at the nozzle exit. The subharmonic, which is conditional to vortex merging, must have a period equal to the advection time from the nozzle lip to the pairing location plus the feedback time.

It was previously shown that, for impinging jet-flow-field, turbulence intensities and mean velocities differed from those of a free jet only within a distance of less than about two nozzle diameters from the plate. Marked increases in turbulence intensities were measured in the free stream close to the surface [7]. Others used a smoke-wire flow visualization technique to investigate flow structures of unforced free and impinging circular jets, concluding that the presence of an impingement plate does not affect upstream vortical structures [8]. Large-scale toroidal vortices that were incident on the plate induced consecutive ring-shaped wall eddies.

A prior work documented that stagnation-point heat transfer in axisymmetric submerged jets is enhanced by a surface renewal effect produced by the impingement of large-scale structures on the boundary layer [9]. The maximum Nusselt number corresponded to flow condi-

tions where turbulent surface renewal had maximum frequency. One of the few prior experimental studies on heat transfer to pulsating jets found that time-averaged Nusselt numbers were independent of pulse amplitude, frequency, and waveform for a pulsating circular air jet $St_w < 10^{-2}$ [10]. More recently, pulsations in unsubmerged planar water jets led to decreases in local, time-averaged Nusselt numbers for $0.012 < St_w < 0.144$ and pulse amplitudes higher than 40 % [11], or to increases of up to 100 % for intermittent jets $St_w > 0.26$ [12]. The reductions were attributed to nonlinear dynamical responses of momentum and heat transports within the boundary layers to the flow pulsations, whereas the enhancements were due to the thinner boundary layers resulted from the periodic restart of the flow.

The causative relationship between the flow and the heat flux temporal variations is commonly characterized by the coherence function. This function compares the amplitude and phase of each of the Fourier components of the signals. It, therefore, tests for a linear relationship between the two signals and provides a way of quantifying the correlation between signals. The maximum possible coherence is defined as unity. Previous studies suggest that the coherence between the velocity and heat flux signals increases with the degree of order in the flow. For example, it was found a maximum coherence function of 0.3 between the fluctuations in the velocity outside the stagnation boundary layer of an unforced jet flow and the surface heat flux fluctuations [13]. By contrast, the heat transfer fluctuations and the oscillations caused by vortex shedding in the wake of a cylinder had a maximum coherence of 0.9 at the shedding frequency [14].

In light of changes observed in the flow structures of submerged jets and given that prior studies at higher Strouhal numbers have involved only unsubmerged jets where vortex structures of *figure 1* do not arise, it was deemed appropriate to investigate the flow structure and heat transfer performances when flow pulsations are induced in the incident jet velocity. A single frequency (f_{ex}) pulsation of amplitude A_N at the nozzle exit was superimposed on a forced subsonic planar air jet with an initially low (below 2 %) turbulence level. Experiments were performed for Reynolds numbers of 1 000, 5 500, and 11 000. Pulsation frequencies ranged from 0 Hz to 82 Hz, corresponding to Strouhal numbers below 0.13. The pulse amplitude at the nozzle exit was varied from 0 to 50 % of the mean flow velocity. The measured surface heat flux ranged from 0.3 to 0.9 $W{\cdot}cm^{-2}$, and corresponded to surface temperatures between 50 °C and 96 °C. Air jets were produced at ambient pressure and temperature.

The flow dynamics was studied mainly for a free (non-impinging) jet. However, significant information about the flow field in the near-surface region was obtained from heat transfer measurements taken when the jet impinged on the heated plate. The nozzle-to-plate separation distances were kept in the range from 3 to 10 nozzle widths, where the free jet measurements indicated a clear preservation of the flow two-dimensionality and the least degradation of the forced periodic fluid motion.

2. EXPERIMENTAL APPARATUS AND PROCEDURES

A schematic of the experimental apparatus is shown in *figure 2*. Filtered and dehumidified air was directed to an air reservoir via a pressure regulator. Air flow to the nozzle was partitioned through a parallel flow network by one of two needle valves. In one branch of this network, air from the reservoir flowed with little restriction to the plenum box of the nozzle. In the other branch, the air flow was periodically interrupted by the continuous rotation of a ball valve. Rotation was provided by a variable-speed direct-current motor. A position indicator was installed on the motor shaft, such as the position of the ball valve and the phase within the pulse cycle were detectable from a series of electrical spikes. A specific pulse amplitude was obtained by adjusting with the needle valves the amount of flow through each branch of the network. The air reservoir and damping chambers promoted a nearly sinusoidal pulse waveform. Thermal anemometry equipment was calibrated in place with a separate Pitot tube.

A convergent geometry was used and air flow was provided symmetrically to a plenum box with internal baffle plates and a honeycomb flow element. The nozzle had an inlet opening of 25 mm × 50 mm and an outlet opening of 5 mm × 50 mm. A 70 mm long convergent section was followed by a straight transition section 5 mm in length. A 120 mm × 100 mm extension plate was attached flush to the nozzle opening. The plenum box was attached to a traversing mechanism to allow different nozzle-to-plate separation distances. The jets discharged upward onto a 5 mm thick aluminum nitride (k = 150 $W{\cdot}m^{-1}{\cdot}K^{-1}$) ceramic plate that was 100 mm long and 50 mm wide. Discharging the jets upward provided a thermally stable flow to obviate possible influences due to gravity. Heat was provided to the unexposed surface of the ceramic plate by passing electrical current through a thin nickel–chromium foil. The plate and foil were mounted on a phenolic box.

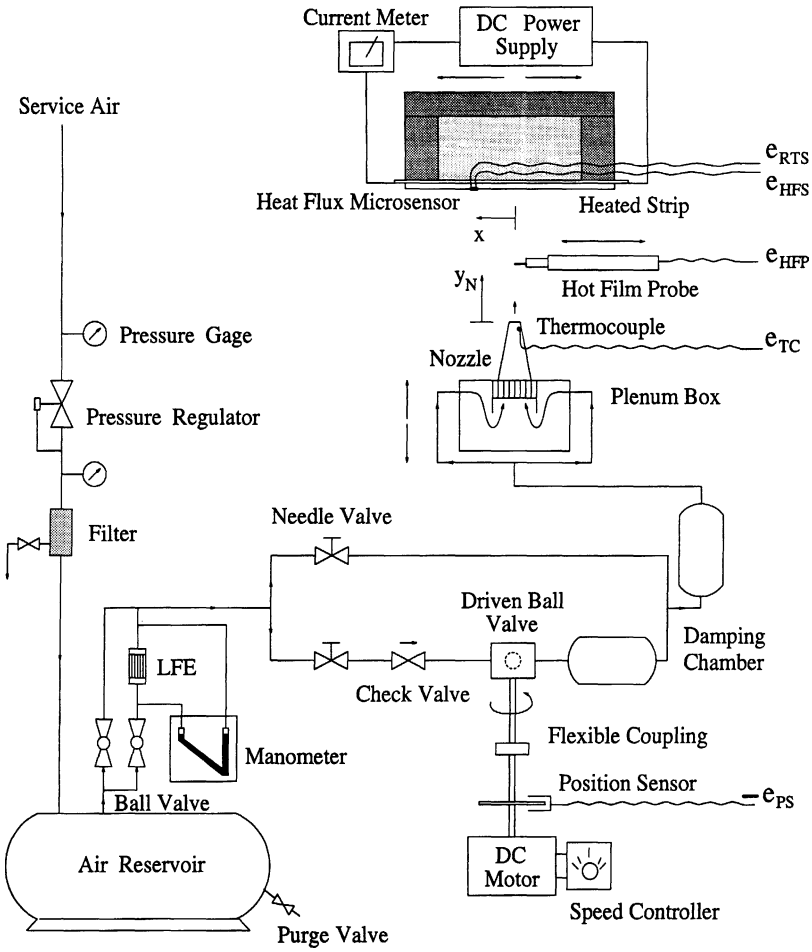

Figure 2. Schematic representation of the experimental apparatus.

Local heat flux and surface temperature signals were obtained with a 2 μm thick microsensor of 20 μs time response, manufactured by Vatell Corporation (Blacksburg, Virginia) for the specific purpose of this study. The microsensor was fabricated directly onto the ceramic plate and consisted of a thin-film heat flux sensor, formed of 250 nickel–nichrome thermocouples placed in series, and a platinum thin-film as a resistance temperature sensor. The sensors were oriented parallel to the length of the nozzle slot opening, covering a total area of 1.2 mm × 25 mm. A detailed description of the sensor and its calibration procedure has been given by the authors in a prior paper [15]. The sensor was placed at an off-center location to allow lateral measurements by moving the phenolic box.

A single sensor thermal anemometer, operated in the constant temperature mode, was used for jet velocity measurements. The anemometer probe consisted of a cylindrical hot-film sensor manufactured by TSI (Model 1210-20). The sensor was mounted in an end-flow configuration with the hot-film axis parallel to a plane normal to the jet (*figure 2*). The probe extension was mounted on a traversing mechanism with three degrees of freedom so that the sensor could be located to within 0.25 mm of a desired location in the flow field.

The investigation of the periodic flow-fields and large flow structures has required a special theoretical approach. As commonly done, the instantaneous flow field was decomposed to uncorrelated mean (time averaged) component $\overline{V}$, periodic component $\widetilde{V}$ and turbulent component V':

$$V(t) = \overline{V} + \widetilde{V}(t) + V'(t) \tag{1}$$

Direct time-averaging of all instantaneous velocity measurements determined $\overline{V}$. In order to separate the turbulent component from the periodic one, measurements must be statistically averaged over many pulsation cycles. The previously developed ensemble-averaging technique [16] was used for this purpose. Details of how this technique has been applied to the present study were included in a past publication of the authors [15]. The ensemble-averaging yielded the velocity waveform $\langle V(t)\rangle$.

Since ensemble-averages are identical to time-averages for homogeneous and isotropic fluctuations in stationary functions, the cyclic or periodic velocity of zero mean was defined as

$$\widetilde{V}(t) = \langle V(t)\rangle - \overline{V} \tag{2}$$

The random turbulent velocity fluctuations were assumed to be statistically independent of the periodic velocity fluctuations. The flow unsteadiness was characterized in terms of the turbulence intensity level *Tu* and the pulsation amplitude *A*, defined after Evans [16]

$$Tu = \frac{1}{\overline{V}}\sqrt{\frac{1}{nN}\sum_{k=1}^{nN} V_k'^2} \quad \text{and} \tag{3a}$$

$$A = \frac{1}{\overline{V}}\sqrt{\frac{1}{n}\sum_{i=1}^{n} \widetilde{V}_i^2} \tag{3b}$$

In the equations above, n represents the number of velocity readings per cycle and N represents the number of complete cycles during which the velocity data was recorded.

The ensemble averaging technique was also applied to instantaneous surface heat flux and surface temperature measurements made with the microsensor. The associated waveform amplitudes A_T and A_q were computed as root-mean-squares of the ensemble-average data and were defined as percentages of the mean values. Convective heat transfer coefficients were determined directly from instantaneous data of surface heat flux, surface temperature, and jet temperature at the nozzle opening. In these calculations, the net radiative heat flux from the impingement surface was subtracted from the total heat flux to obtain the heat flux due to convection. As defined in practical applications, the time-averaged Nusselt number was based on nozzle width, time-averaged heat flux, and time-averaged temperature difference:

$$Nu_{\text{avg}} = \frac{\bar{q}_{\text{s}}}{\overline{T}_{\text{s}} - T_{\text{j}}}\,\frac{w}{k(\overline{T}_{\text{f}})} \tag{4}$$

The high thermal conductivity of the aluminum nitride plate yielded a nearly uniform and essentially constant surface temperature ($A_T < 1\,\%$). Both the steady and pulsating flow results of this study thereby pertained closely to a constant and uniform surface temperature heating condition. Since the incident jet temperature was also constant, the Nusselt number variations reflected essentially the actual heat flux variations and the two variables were similar from the dynamical point of view.

The sampling rate was set at 4 kHz/channel or higher, such as to record about $n = 100$ readings for each pulse cycle and channel over about $N = 600$ cycles. Once the desired pulse amplitude and frequency were set, flow data were recorded. The anemometer probe was then removed and heat transfer measurements were recorded to eliminate possible disturbances caused by the probe. All measurements were continuously synchronized by the electrical pulses generated by the shaft position sensor; this has allowed subsequent association of instantaneous flow and heat transfer readings.

Uncertainties in flow velocities and heat transfer coefficients were estimated according to common techniques [17, 18]. The relative error in local Nusselt number ranged from 9.5 % to 12 % with increasing Reynolds number. Uncertainties in measured velocities and Reynolds numbers varied from 4 % to 7 % with decreasing velocity. Repeatability (i.e., run-to-run variations) of all results was within 2 %. Measured stagnation region Nusselt numbers for steady jets with $Re_w = 1\,000$ and $H/w = 3$ were within 5 % of the theoretical laminar solution of Evans [19]. Such jets had $Tu_{\text{N}} < 1\,\%$ and the potential core incident on the surface.

3. RESULTS

3.1. Flow pulse evolution along centerline

A non-impinging jet is used to illustrate the streamwise pulse evolution. The propagation of the pulse as a wave of variable amplitude is most apparent in the ensemble-averaged profiles of the centerline velocity in *figure 3*. The ensemble-averaged profiles were scaled with the nozzle exit velocity in order to emphasize the relative magnitude of the fluctuations. The ensemble-averaging technique removed the random fluctuations from the instantaneous velocity data but preserved the fluctuations from the organized flow motion. For the sake of clarity, only four instants of time equally separated over one forcing period $1/f_{\text{ex}}$ were chosen.

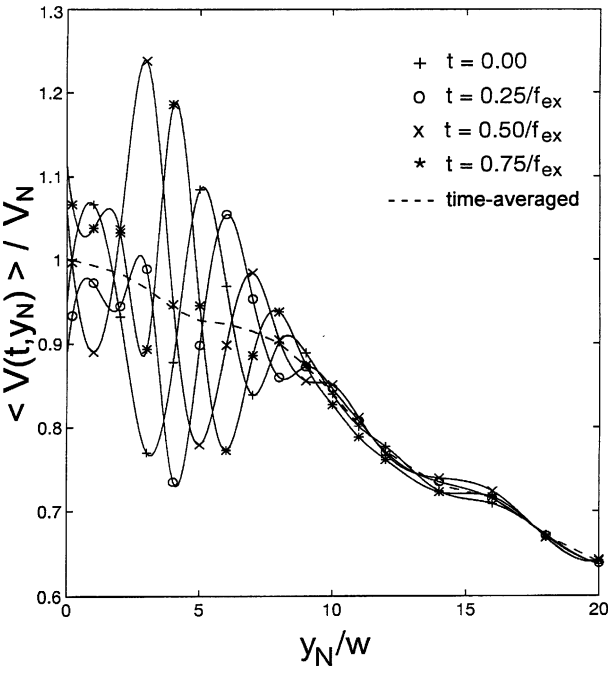

Figure 3. Ensemble-averaged profiles of the centerline velocity. $Re_w = 1\,000$, $A_N = 5\%$ and $f_{ex} = 82$ Hz ($St_w = 0.13$).

The distance between two subsequent velocity maxima or minima represents a measure of local instantaneous wavelengths. The plotted curves show the coexistence of small and large wavelengths over the first two nozzle widths from the jet origin. Beyond $y_N/w = 2$, the pulses extended over about two large wavelengths before degrading into random fluctuations at $y_N/w \cong 9$. The time-averaged centerline velocity in *figure 3* indicates a core region shorter than four nozzle widths, which was the length of a steady (unforced) jet core. Moreover, it is apparent the pulse amplification in the near nozzle-field, where the mean motion fed the periodic motion.

Figure 4 presents the streamwise phase shift of the flow pulse, referenced to the nozzle exit. A complete cycle corresponds to a phase difference $\Delta\varphi = 1$ between the periodic velocity at the beginning and end of the pulse [i.e., $\varphi(t + 1/f_{ex}) - \varphi(t) = 1$]. The phase difference between two velocity signals was computed as the number of data points between the minima minimorum of the two waveforms (periodic velocity components), divided by the total number of readings per cycle. The phase difference thus defined is meaningful as long as the waveforms are based on the same fundamental frequency (here, f_{ex}). Note that the data sampling rate was kept constant and that the cycles were continuously synchronized with the aid of the ball valve position sensor

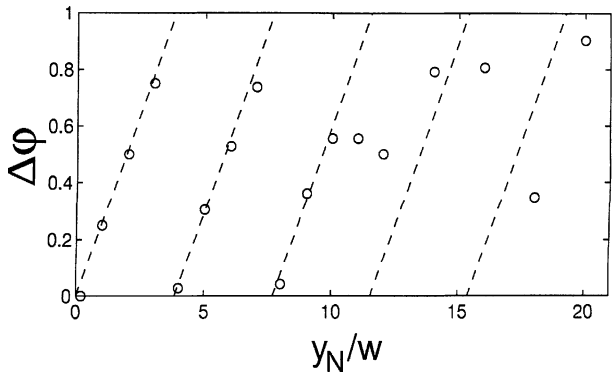

Figure 4. Streamwise phase-shift in flow pulse waveform for conditions of *figure 3*.

installed on the motor shaft (*figure 2*). Therefore, the streamwise phase shift of the flow pulse, referenced to the nozzle exit, indicates the difference in the developing stages of the local pulse of frequency f_{ex}. It thereby provides information about the travel of the forced pulse in the flow-field. The distance traveled by the pulse during one cycle is the distance between two subsequent in-phase velocities and corresponds to one wavelength λ (i.e., λ corresponds to $\Delta\varphi = 1$). For downstream locations where the forced pulse of frequency f_{ex} was significant, *figures 3* and *4* indicate a unique wavelength $\lambda/w \cong 3.9$. The traveling speed of the pulse was computed as $c = \lambda f_{ex} \approx 1.6$ m·s^{-1}, which was half of the nozzle exit velocity V_N ($= Re_w \nu/w$). The randomness of data points for $y_N/w > 10$ in *figure 4* relates to the pulse destruction shown in *figure 3* at the same downstream locations. On the other hand, once the forcing frequency lost its dominance and the velocity waveform resembled less and less to a sine-wave, the phase shift defined as above became ambiguous.

It is noteworthy the agreement of the results with previous studies on jet flows. In an unforced planar submerged water jet and in the vortex region upstream of the first merging point, Rockwell and Nicholls [2] found that the Strouhal number and wavelength associated with the natural vortex passages correlated with $(Re_w)^{0.5}$ and $(Re_w)^{-0.5}$, respectively, such that $c = \lambda f = 0.528 V_N$. As opposed to natural large vortices, in the presence of an external periodical disturbance, the large flow structures have the frequency fixed by forcing. Ho and Huang [5] showed that the forced large structures, formed within the mixing layers at $1/f_{ex}$ time intervals, traveled through the flow as huge eddies, with a constant advection velocity. Since their frequency equaled f_{ex}, it follows that their associated wavelength and size decreased with increasing forcing frequency.

The results in *figure 4* indicate that the slope of the lines to which the data align is equal to about $2St_w$. An approximate relation for calculating the streamwise wavelength in the near nozzle region is then given by

$$\frac{\lambda}{w} = \frac{1}{2St_w} \tag{5}$$

Since the phase-shift variation repeated periodically after each streamwise wavelength (*figure 3*), an estimate of the downstream phase-shift in pulse centerline velocity resulted as

$$\Delta\varphi = 2St_w\left(\frac{y_N}{w} - n\,\frac{\lambda}{w}\right) \tag{6}$$

where $n = 0, 1, 2, 3, \ldots$. Equation (6) is plotted in *figure 4* with a dashed line for comparison with experimental data. Notably, past works associated the wavelength with the subharmonic of one half forcing frequency and the feedback process. According to the feedback requirements, the vortex mergings/pairings must take place at integer numbers of wavelength. For example, it was reported that the first and second mergings happen respectively at $N\lambda$ and $2N\lambda$ from the origin, where $N = 4$ for mixing layers [5] and $N = 2$ for jets [20]. *Figure 3* shows that the flow pulse increased over one wavelength ($0 < y_N/w < 4$) and decayed over the next ($4 < y_N/w < 8$). This result suggests that the first structure merging began at $y_N/w = \lambda$ and was completed at $y_N/w = 2\lambda$.

Investigation was further extended by analyzing the downstream centerline velocity auto-correlation and power spectra, as commonly in disturbed flows [21]. Note that these tools were applied to the fluctuating (periodic plus turbulent) velocity signals and not only to the periodic components as did the phase shifting. Velocity autocorrelation and power spectra revealed new aspects of the flow structure properties, which were dimmed in the process of ensemble-averaging and thus in the waveform phase shift. Results indicated that, from $y_N/w = 0.2$ to $y_N/w = 7$, small structures of frequency f_{ex} coexisted with large structures of frequency $0.5f_{ex}$. Beyond $y_N/w = 8$, only the lower frequency was displayed. At $y_N/w = 20$, velocity auto-correlation indicated no periodicity in the flow, whereas the power spectrum still displayed a peak frequency equal to $f_{ex}/6$. Though very weak, the pulse was still evident in the turbulent region of the jet.

The length scale of large-scale structures may be estimated by multiplying the structure convective velocity with the time period of the structure motion. The constant wavelength indicated in *figures 3* and *4* for $0 < y_N/w < 10$ suggests that the structures of f_{ex} were advected twice as fast than the enlarged structures of $0.5f_{ex}$. This observation is supported by the mechanism of vortex pairing documented by Rockwell and Niccolls [2]. The new smaller vortices traveled faster and reached the slower large vortices with which eventually became coalescent (*figure 1*). Thomas and Goldschmidt [22] associated the characteristic structural frequency halving in a turbulent jet, not only with the merging of shear layers at the end of the potential core, but also with the formation of symmetric structural modes with respect to the jet centerline. This past result suggests that the jet investigated in *figure 3* had a symmetrical structure.

3.2. Flow pulse influence on instantaneous heat transfer distribution

Time-dependent heat transfer distributions in a pulsed impinging jet represent a novelty in the engineering field. When a flow like the one in *figure 3* impinges on a heated surface, it may induce fluctuations in the surface heat flux and surface temperature. Instantaneous scaled distributions of heat flux and corresponding Nusselt number are similar according to Newton's law of cooling so long as the jet and surface temperature are essentially constant. This was the case of the present experiments. Consequently, the periodic local Nusselt number may be approximated with the corresponding periodic heat flux.

Figure 5 illustrates instantaneous Nusselt number distributions for $St_w = 0.106$. The local Nusselt number ensemble averages were scaled with the time-averaged Nusselt number at the stagnation line to emphasize the relative magnitude of instantaneous fluctuations. For the sake of clarity, distributions are illustrated only for four instants of time equally separated over one forcing period $1/f_{ex}$. The local time-averaged Nusselt numbers scaled with the time-averaged stagnation line Nusselt number are shown for comparison. Instantaneous Nusselt number displays large departures from its time-average in the stagnation region and wall–jet region. The fluctuation amplitudes reached maximum values between four and six nozzle widths from the stagnation line, after which they decayed by viscous dissipation effects. The distance between two subsequent maxima or minima of the same wave represents the local wavelength λ_x at that instant of time.

Power spectra of the heat flux signal gave information about the coherent structure dynamics. Roughly, due

to the conservation of the kinetic moment in a coherent structure, the forcing (pulsation) frequency harmonics nf_{ex} (n—an integer number) are related to broken structures of size w/n, while the forcing frequency subharmonics f_{ex}/n are related to enlarged structures of size nw. The big structures may have been caused by mergings of two or more smaller structures or by flow spread after the pressure gradient vanished. The spatial sequence of heat flux power spectra indicated for $x/w < 8$ a clear dominance of the flow pulses at the forcing frequency (as evident also in *figure 5*). However, around $x/w = 8$, the heat flux power spectra started displaying a dominant frequency at $0.5\,f_{ex}$. In the entire wall–jet region, besides the peak frequency, the presence of harmonics and subharmonics of small amplitudes suggested a continuous coherent structure redistribution among sizes until complete destruction of the organized motion beyond $x/w = 10$.

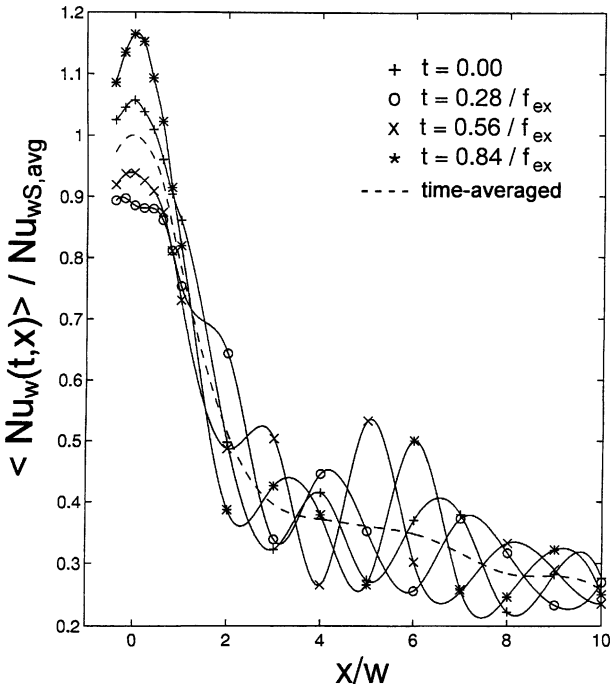

Figure 5. Instantaneous Nusselt number distribution. $Re_w = 1\,000$, $f_{ex} = 80$ Hz ($St_w = 0.106$), $A_N = 5\%$, and $H/w = 5$.

3.3. Correlation of flow pulse and instantaneous heat transfer along the surface

The instantaneous heat flux data brings information about the heat transfer driving mechanisms as well as flow-field structural characteristics near the impinging surface. In *figure 6a*, the incident velocity and stagnation line ($x = 0$ in *figure 2*) heat flux signals produced a coherence estimate of unity at both f_{ex} and $2\,f_{ex}$ and had an average of 0.65 over the entire frequency content. Results suggest that the surface heat flux fluctuations were driven by the flow velocity fluctuations in the plane of impingement and that the driving relationship was stronger at frequencies related to the forcing.

Similar to stagnation region, there is a degree of coherence between the local heat flux and the local freestream velocity (i.e., velocity outside the hydrodynamic boundary layer). *Figure 6b* illustrates a case where the coherence function estimate of the local heat flux and freestream velocity signals had a maximum value of 0.98 at the forcing frequency and an average of 0.42 over the entire frequency content. The lower coherence level compared to the stagnation line in *figure 6a* was caused by freestream turbulence effects on heat transfer [15]. Previous studies [13, 14] showed that any randomness present in two dependent signals lowers their coherence.

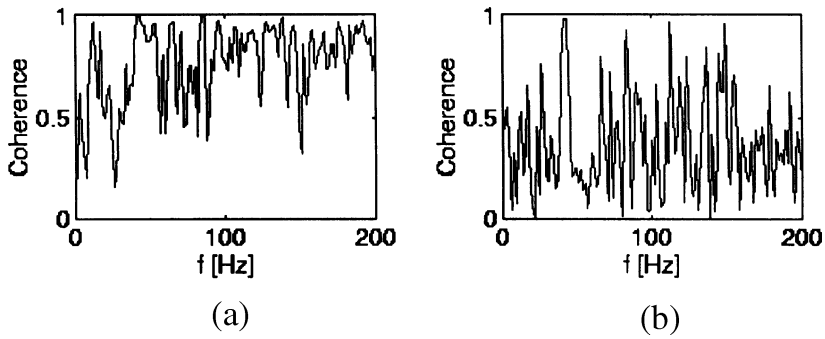

Figure 6. Coherence function estimates between velocity and surface heat flux signals. (a) $Re_w = 1\,000$, $f_{ex} = 41$ Hz, $A_N = 16\%$, $H/w = 5$, and $x/w = 0$ (velocity probe at $y_N/w = 4.0$). (b) $Re_w = 5\,500$, $f_{ex} = 41$ Hz, $A_N = 15\%$, $H/w = 5$, and $x/w = 3$ (velocity probe at $y_N/w = 4.5$).

Experimental results showed that, under same pulsed flow conditions, the associated ensemble-averaged heat fluxes assumed wave-type variations. The waveforms had a similar shape but their amplitude and phase varied from those of the nozzle-exit velocity with nozzle-to-plate distance. Such surface heat flux variations gave information about the driving coherent flow structures present close to the surface, where the intrusion of any probe would disturb the flow characteristics.

The surface heat flux periodic component is expected to be phase-shifted from the nozzle exit velocity waveform but almost in phase with the velocity waveform close to the surface. *Figure 7* presents for $0.003 < St_w < 0.106$ the phase shift between the nozzle exit velocity waveform and the stagnation line ($x = 0$ in *figure 2*) heat flux wave-variation with nozzle-to-plate distance. Based on the data cyclic synchronization and the constant sampling rate, the phase difference between the two signals was computed in the same way as discussed in relation to *figure 4*. Equation (6) showing the incident flow pulse phase is plotted in this figure for comparison. For high Strouhal numbers or small separation distances, the agreement of experimental data with equation (6) is remarkable. The data departed from equation (6) at higher nozzle-to-plate distances and for decreasing Strouhal numbers and increasing pulse amplitudes.

Previous works [23, 24] reported a phase lag in stagnation heat transfer compared to the freestream fluctuations but the lag was more pronounced at higher frequencies. This result suggests that the deviations of data from equation (6), shown in *figure 7* for $St_w \leq 0.054$ and $A_N > 5\,\%$, are not related to a delay in heat transfer relative to the flow but may be caused by the interaction between the surface and the impinging large structures associated with large pulse amplitudes. However, the pulse decay was shown to be faster at higher nozzle exit pulse amplitudes and same Strouhal number [15], which is consistent with the deviations shown in *figure 7*. Results suggest thus that the stagnation line heat flux and the flow pulse in the impinging plane were essentially in phase.

Based on results of *figure 6b*, the phase variation of heat flux ensemble-average with distance from the stagnation line gives significant information about flow pulse propagation away from the stagnation line (i.e., in the so called wall–jet region). *Figure 8* presents the phase differ-

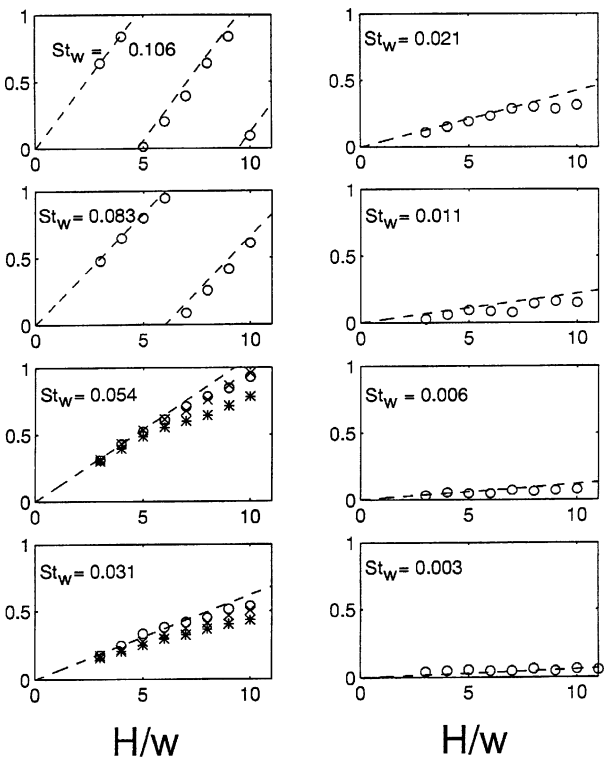

Figure 7. Phase-shift $\Delta\varphi$ between the nozzle-exit periodic velocity and the stagnation line ($x = 0$) periodic heat flux: --- equation (6), $\circ$ $A_N = 5\,\%$, $\times$ $A_N = 25\,\%$, $*$ $A_N = 50\,\%$.

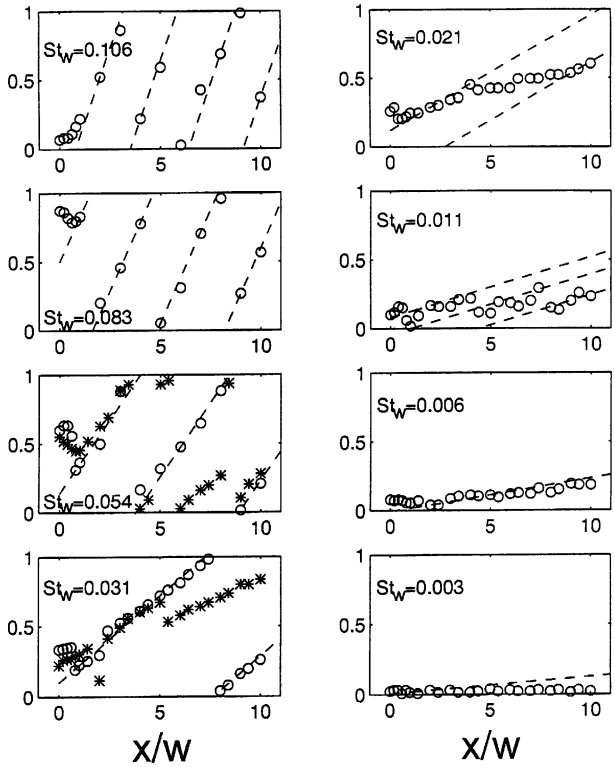

Figure 8. Phase-shift $\Delta\varphi$ between the nozzle-exit periodic velocity and the local periodic heat flux for $H/w = 5$: --- equation (8), $\circ$ $A_N = 5\,\%$, $*$ $A_N = 50\,\%$.

ence $\Delta\varphi$ between the nozzle-exit jet velocity waveform and surface heat flux wave-type variation along the plate. At the stagnation line, $\Delta\varphi_S$ corresponds to the value indicated in *figure 7* for the same Strouhal number. The phase differences are shown to vary inconsistently over a short distance Δx from the stagnation line, whereas for $x > \Delta x$ some trends are apparent. Compared to the trends shown at the stagnation line (*figure 7*), the experimental data points in *figure 8* align to straight lines of slope $4St_w$ instead of $2St_w$.

Following the same reasoning as for equations (5) and (6), the associated wavelength and phase-shift along the plate (in the x-direction, see *figure 2*) may be approximated with the equations

$$\frac{\lambda_x}{w} = \frac{1}{2St_w} \tag{7}$$

and

$$\Delta\varphi_x = 4St_w\left(\frac{x-\Delta x}{w} - n\,\frac{\lambda_x}{w}\right) + \Delta\varphi_S \tag{8}$$

where n is a positive integer. Equation (8) is plotted in *figure 8* next to experimental data for comparison. The corresponding dashed lines have a period of unity, based on the fact that a full forcing cycle was associated with $\Delta\varphi = 1$. However, this rule is disobeyed in the panels corresponding to $St_w = 0.021$ and 0.011, just to emphasize that some data points seem to still align to a shifted periodicity. This result may be attributed to some structure interactions and/or flow instabilities. In addition, the coexistence of structures of different frequencies may cause errors in the computation of the phase difference.

The apparent halving of pulse wavelength λ_x ($= c_x \cdot f_{ex}$) in the wall jet region is remarkable. The average advection velocity inside the boundary layer is roughly half-freestream velocity and the freestream velocity is about equal to the incident jet velocity V. Ho and Huang [5] reported that the advection velocity of large structures in a mixing layer formed between two planar flows of different velocities was the arithmetic average velocity. On the other hand, the dominant frequency might change in the wall jet region from f_{ex} to $2f_{ex}$ due to the broken structures of size equal to about one half the nozzle width indicated near the surface by previous experimental studies [25, 26]. It is also possible that a superposition of waves existed at both f_{ex} and $2f_{ex}$. This is suggested by the instabilities shown in *figure 8* for $St_w > 0.083$, when the experimental data align subsequently to lines of higher and lower slope. On average, the instantaneous wavelength value indicated in *figure 8* complies with equation (7). The apparent variations were caused by the complex frequency content in the driving flow-field and by limited number of data points as well.

Results indicated that the heat flux departures from its time-average were smaller than the corresponding velocity fluctuations. This effect is supported by the common correlation $Nu \sim Re^m$, where $m = 0.5$ at stagnation line and $0.5 < m < 0.8$ away from the stagnation line. Under constant surface temperature condition, a quasi-steady approximation of the system behavior suggests that $(1 + A_q) \propto (1 + A)^m$. The approximate feature of the above relationship comes from the nonlinear effects related to transients [24] and from the different turbulence levels associated with pulsed impinging jet flows [15].

Surface heat flux measurements at the stagnation line ($x = 0$ in *figure 2*) showed that the amplitude ratio A_q/A_N decreased with decreasing forcing frequency and increasing nozzle-exit pulse amplitude. Similarly, flow measurements in the non-impinging pulsed jets indicated that the centerline pulse amplitude A had smaller departures from the nozzle exit value A_N with decreasing Strouhal number and increasing A_N [15]. These results suggest that the heat flux amplitude correlated with the flow pulse amplitude in the plane of impingement in the manner discussed above. Away from the stagnation line, the heat flux fluctuations exhibited an increase in amplitude, as the flow spread at zero pressure gradient, being more pronounced at higher Strouhal numbers and lower nozzle-exit pulse amplitude.

Heat flux frequency spectra at the stagnation line suggested that pulses of low amplitude produced increased turbulent motion in the plane of impingement. By contrast, pulses of high amplitude produced broken structures of frequency nf_{ex} at the surface. This result is supported by the inhibited turbulence development in non-impinging pulsed jets for higher A_N [15].

3.4. Influence of flow pulse amplitude and frequency on time-averaged heat transfer

A detailed discussion of time-averaged heat transfer alterations in pulsating air jet flows is included in prior publications. For the sake of completeness, a few results are briefly presented here. For small nozzle-to-plate distances, high Strouhal numbers and high pulse amplitude, the Nusselt number was higher than for the steady-jet value. For example, it was higher with 12 %

for $Re_w = 1\,000$, $H/w = 3$, $St_w = 0.054$ and $A_N = 50\,\%$, which exceeds by far the experimental repeatability of 2 %. This result suggests that the large coherent flow structures associated with a high-amplitude high-frequency flow pulse might have increased Nusselt number at stagnation line by surface renewal effects, as previously documented by Kataoka et al. [9] in unforced impinging flows. At Strouhal numbers below 0.05 and pulse amplitudes lower than 17 %, decreases of up to 8 % or similar values with the steady-jet ones were recorded. The former effect was associated with a quasi-steady behavior of the flow. The decrease in heat transfer was attributed to nonlinear dynamics effects, as documented in a previous theoretical work [27]. The nonlinear dynamic effect reflects that the disturbances associated with flow pulsation do not allow momentum and energy transfer to equilibrate within the boundary layers.

Results indicated that the most important pulse effects corresponded to high values of the product $St_w A_N$. This combined parameter has meaning in all periodically disturbed flows. As shown by Reynolds and Hussain [28], the transient term in the ensemble-averaged Navier–Stokes equation for the periodic velocity component has the order of magnitude equal to the product $St_w A_N$. Unfortunately, high pulse amplitudes could neither be produced in high Reynolds jets nor be associated with high frequency flow pulses due to fluid inertia and compressibility effects.

The authors of the present paper found a low Reynolds number influence on the pulsed flow properties (i.e., in addition to that on the steady jets). The general flow properties were largely determined by the behavior of the coherent structures, which are essentially inviscid phenomena. Likewise, work performed by Broze and Hussain [29] on forced transitional circular air jets concluded that the flow structural characteristics were independent of Reynolds number as long as an initially laminar, top-hat profile was maintained at the nozzle exit.

A sample of Nusselt number distributions is shown in *figure 9*. Increased freestream turbulence that occurred for $A_N > 5\,\%$ in *figure 9a* may be responsible for small, local increases. Increases are most pronounced in the wall–jet region ($x/w > 2$), where the favorable pressure gradient subsides and the flow becomes unstable due to viscous effects. Remarkable is the increase in Nusselt number over the steady-state case by 35 % around $x/w = 6$ to 80 % at $x/w = 10$, for $A_N = 50\,\%$. An earlier transition to turbulence is also noted in *figure 9b* at the higher Reynolds number $Re_w = 5\,500$ and with $St_w = 0.011$ and a pulse amplitude of 17 %. Beyond two nozzle widths away from the stagnation line, the local Nusselt number for $A_N = 17\,\%$ became up to 25 % higher compared to the steady-state distribution. Flow measurements indicated an increased freestream turbulence that might have been carried near the surface. It destabilized the hydrodynamic boundary layer at locations where the favorable pressure subsided ($x/w > 2$). The above mentioned heat transfer enhancements may therefore be attributed to increased freestream turbulence intensities caused by the flow pulse. *Figure 9c* shows for $Re_w = 11\,000$ and $St_w = 0.003$ no significant change in heat transfer characteristics for A_N as high as 12 %. This result suggests that the pulse was not strong enough to trigger natural instabilities. Transition to fully turbulent flow in the wall jet region developed as in the unperturbed flow.

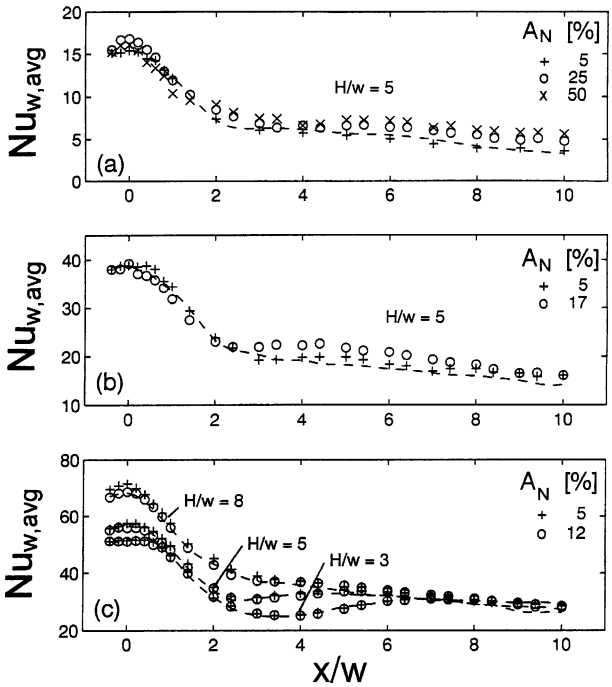

Figure 9. Influence of pulse amplitude on time-averaged Nusselt number distribution: --- steady jet. (a) $Re_w = 1\,000$, $f_{ex} = 41$ Hz, $St_w = 0.054$, (b) $Re_w = 5\,500$, $f_{ex} = 41$ Hz, $St_w = 0.011$, (c) $Re_w = 11\,000$, $f_{ex} = 23$ Hz, $St_w = 0.003$.

4. CONCLUSIONS

The frequency, phase and amplitude in heat flux fluctuations were shown to relate to the flow velocity at the impingement plane. Using an extremely thin heat flux microsensor, heat flux measurements were used in return to infer the characteristics of the flow field close to the im-

pinging surface, where any velocity probe would disturb the flow-field. Results indicated that the forcing Strouhal number was an influential parameter that controlled the large scale structure formation (i.e., structure size and frequency) and interaction (i.e., passage frequency, localized merging point), as well as the downstream penetration distance (i.e., propagation wavelength) of the initial perturbation. The wavelength associated with the flow pulse scaled in the free-jet region with $(2St_w)^{-1}$, whereas in the wall–jet region it scaled with $(4St_w)^{-1}$. The presence of the half-forcing frequency in the power spectra of both velocity and surface heat flux signals indicated a merging process of the coherent flow structures formed at the nozzle exit, and, thus, a symmetric structure for the flow field. The broken structures at the impinging surface were associated with frequencies being multiple of the forcing frequency.

Results indicated the parametric conditions for which enhancements or reductions are expected in heat transfer from the impinging surface. Such information may be used in various engineering applications. For example, pulses of high $St_w A_N$ values may enhance cooling of electronic packages by surface renewal effects from the large incident flow structures. The orifices that are currently used in these applications have shorter potential cores but little coherent flow structure under steady-state conditions. On the other hand, pulses of small frequency but high amplitude may diminish heat transfer in gas turbine flows by nonlinear dynamics effects.

Acknowledgement

Support for this work was provided by the National Science Foundation of the United States of America under Grant No. CTS-8918154 and Grant No. CMS-9253640.

REFERENCES

[1] Gutmark E., Wolfstein M., Wygnanski I., The plane turbulent impinging jet, J. Fluid Mech. 88 (4) (1978) 737–756.

[2] Rockwell D.O., Nicholls W.O., Natural breakdown of planar jets, J. Basic. Eng. 94 (1972) 720–728.

[3] Favre-Marinet M., Binder G., Structure des jets pulsants, J. de Mech. 18 (1979) 355–394.

[4] Farrington R.B., Claunch S.D., Infrared imaging of large-amplitude, low-frequency disturbances on a planar jet, AIAA Journal 32 (1994) 317–323.

[5] Ho C.M., Huang L.S., Subharmonics and vortex merging in mixing layers, J. Fluid Mech. 119 (1982) 443–473.

[6] Laufer J., Monkevitz P., AIAA Paper No. 80-0962, 1980.

[7] Donaldson C.D., Snedeker R.S., Margolis D.P., A study of free jet impingement. Part 2. Free jet turbulent structure and impingement heat transfer, J. Fluid Mech. 45 (1971) 477–512.

[8] Popiel C.O., Trass O., Visualization of a free and impinging round jet, Experimental Thermal and Fluid Science (1991) 253–264.

[9] Kataoka K., Suguro M., Degawa H., Maruo K., Mihata I., The effect of surface renewal due to large-scale eddies on jet impingement heat transfer, Int. J. Heat Mass Tran. 30 (1987) 559–567.

[10] Nevins R.G., Ball H.D., Heat transfer between a flat plate and a pulsating impinging jet, in: Proc. of the Nat. Heat Transfer Conf., Boulder, CO, Vol. 60, 1961, pp. 510–516.

[11] Sheriff H., Zumbrunnen D.A., Effect of flow pulsations on the cooling effectiveness of an impinging planar water jet, J. Heat Tran. 116 (1994) 886–895.

[12] Zumbrunnen D.A., Aziz M., Convective heat transfer enhancement due to intermittency in an impinging jet, J. Heat Tran. 115 (1993) 91–98.

[13] Simmons S.G., Hager J.M., Diller T.E., Simultaneous measurements of time-resolved surface heat flux and freestream turbulence at a stagnation point, J. Heat Tran. 2 (1990) 375–380.

[14] Mancuso T., Diller T.E., Time-resolved heat flux measurements in unsteady flow, in: Proc. of the 1991 National Heat Transfer Conference, Vol. HTD-179, 1991, pp. 67–74.

[15] Mladin E.C., Zumbrunnen D.A., Local convective heat transfer to submerged pulsating jets, Int. J. Heat Mass Tran. 40 (14) (1997) 3305–3321.

[16] Evans R.L., Turbulence and unsteadiness measurements downstream of a moving blade, J. Engrg. Power (January 1975) 131–139.

[17] Kline S.J., McClintock F.A., Describing uncertainties in single sample experiments, Mechanical Engineering 75 (1953) 3–8.

[18] Moffat R.J., Describing the uncertainties in experimental results, Experimental Thermal and Fluid Science 1 (1988) 3–17.

[19] Evans H.L., Mass transfer through laminar boundary layers. 7. Further similar solutions to the B-equation for the case $B = 0$, Int. J. Heat Mass Tran. 5 (1962) 35–37.

[20] Gutmark E., Ho C.M., Feedback mechanism in a free jet, The Bulletin of the American Physics Society, Series II 25 (1980) 1102–1112.

[21] Tennekes H., Lumley J.L., A First Course in Turbulence, The MIT Press, Cambridge, 1972.

[22] Thomas F.O., Goldschmidt V.W., Structural characteristics of a developing turbulent planar jet, J. Fluid Mech. 163 (1986) 227–256.

[23] Gorla R.S.R., Jankowski F., Textor D., Periodic boundary layer near an axisymmetric stagnation point on a circular cylinder, Int. J. Heat Fluid Flow 9 (1988) 421–426.

[24] Mladin E.C., Zumbrunnen D.A., Nonlinear dynamics of hydrodynamic and thermal boundary layers in laminar stagnation flows, J. Thermophys. Heat Tran. 8 (1994) 514–523.

[25] Russel P.J., Hatton A.P., Turbulent flow characteristics of an impinging jet, Proceedings Inst. Mechanical Engineers 186 (52) (1972) 635–644.

[26] Menon R., Liburdy J., Impingement Characteristics of a Heated Two-Dimensional Turbulent Jet, ASME WAM, San Francisco, 1989.

[27] Mladin E.C., Zumbrunnen D.A., Dependence of heat transfer to a pulsating stagnation flow on pulse characteristics, J. Thermophys. Heat Tran. 9 (1995) 181–192.

[28] Reynolds W.C., Hussain A.K.M.F., The mechanics of an organized wave in turbulent shear flow. Part 3. Theoretical model and comparison with experiments, J. Fluid Mech. 54–2 (1972) 263–288.

[29] Broze G., Hussain F., Nonlinear dynamics of forced transitional jets: periodic and chaotic attractors, J. Fluid Mech. 263 (1994) 93–132.